

Supporting Information for

Mechanically and Chemically Robust Sandwich-Structured C@Si@C Nanotube Array Li-Ion Battery Anodes

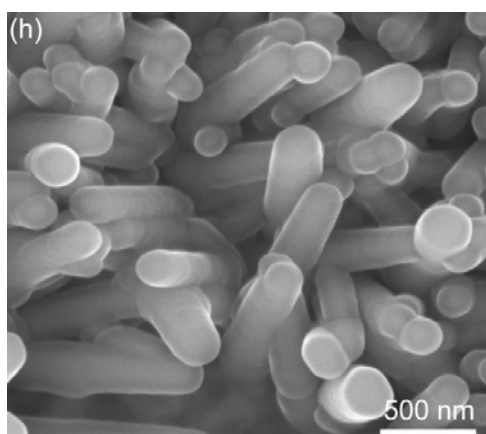
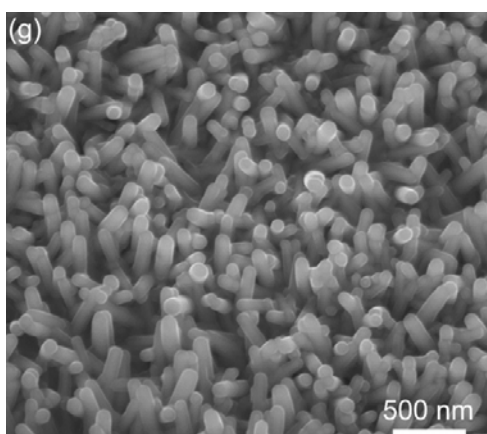
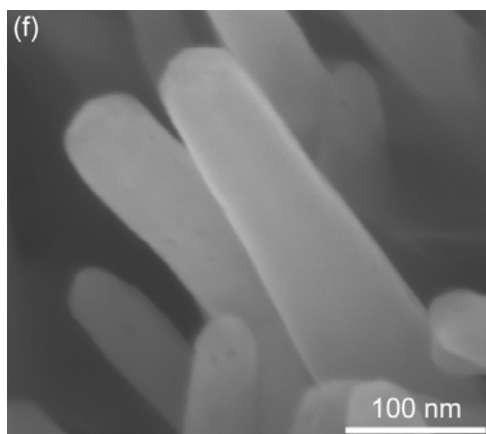
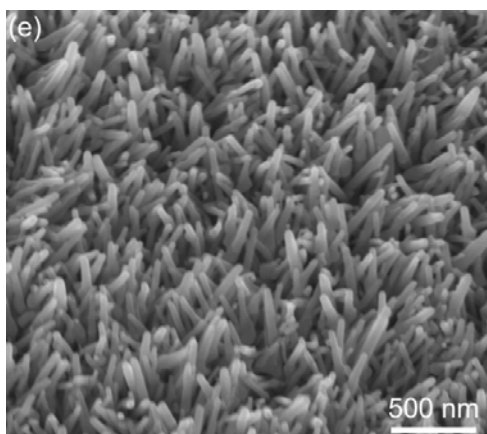
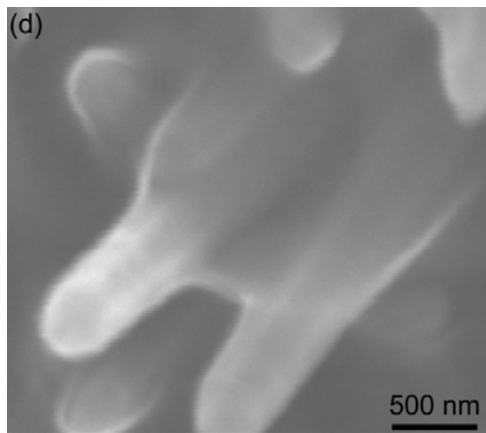
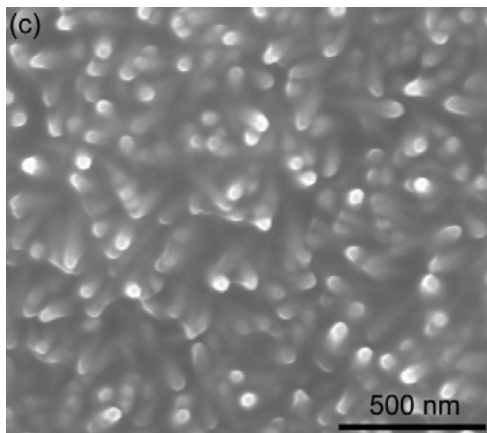
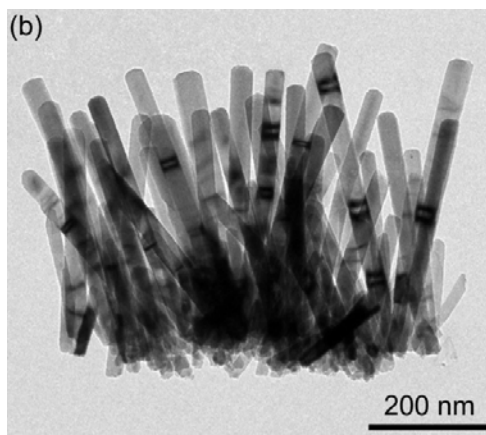
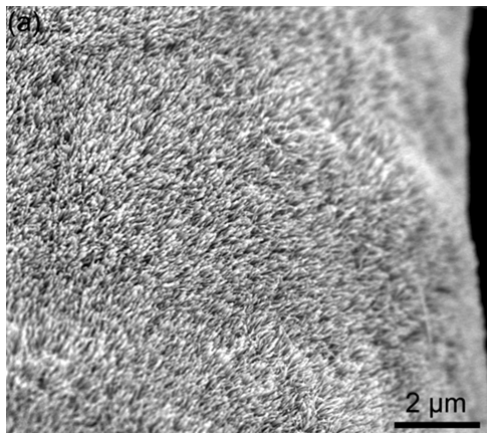
Jinyun Liu,^{†,¶} Nan Li,[‡] Matthew D. Goodman,[†] Hui Gang Zhang,[†] Eric S. Epstein,[†] Bo Huang,[†] Zeng Pan,[†] Jinwoo Kim,[†] Jun Hee Choi,[⊥] Xingjiu Huang,[¶] Jinhuai Liu,[¶] K. Jimmy Hsia,^{‡,§} Shen J. Dillon,[†] and Paul V. Braun^{*,†,‡,§,¶}

[†] Department of Materials Science and Engineering, [‡] Department of Mechanical Sciences and Engineering, [§] Frederick Seitz Materials Research Laboratory, [¶] Beckman Institute for Advanced Science and Technology, University of Illinois at Urbana-Champaign, Urbana, Illinois 61801, USA.

[¶] Research Center for Biomimetic Functional Materials and Sensing Devices, Institute of Intelligent Machines, Chinese Academy of Sciences, Hefei, Anhui 230031, China.

[⊥] Samsung Advanced Institute of Technology, Samsung Electronics, Suwon 443-803, South Korea

* Address correspondence to pbraun@illinois.edu.



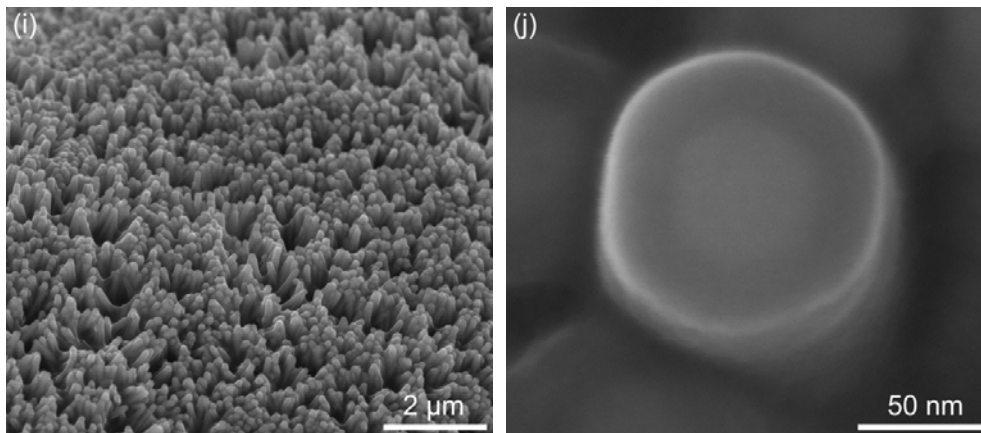


Figure S1. (a) Low-magnification SEM and (b) TEM images of the ZnO nanorod array grown on the Ni foam. (c), (d) SEM images of the carbon precursor-coated ZnO nanorod array (after polymerization in air at 150 °C for 24 h). (e), (f) SEM images of ZnO@C nanorods after carbonization in Ar at 500 °C for 3 h. (g), (h) SEM images of ZnO@C@Si nanorods. (i), (j) SEM images of the ZnO@C@Si@C nanorods (ZnO core has not been etched).

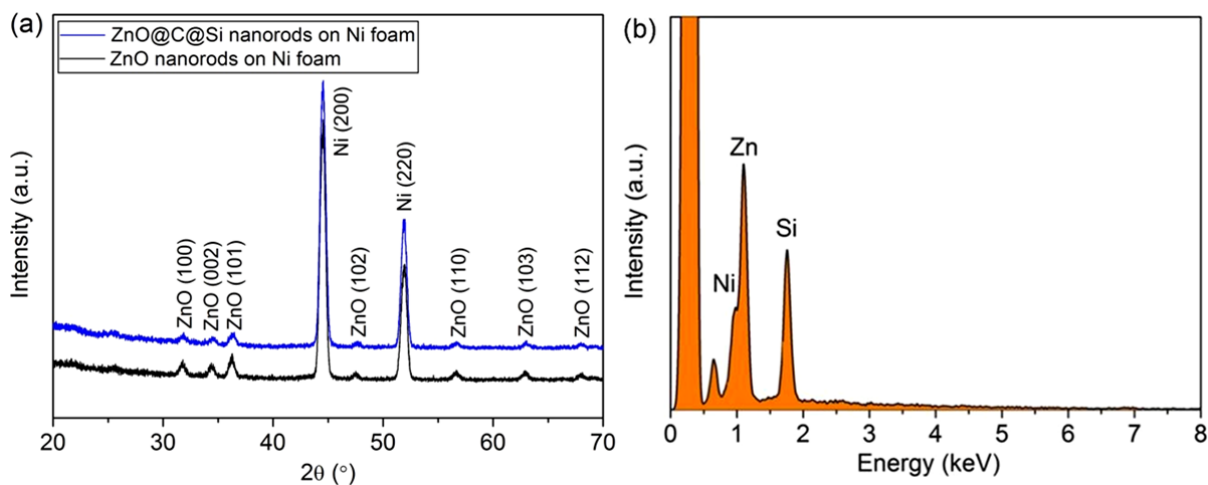


Figure S2. (a) XRD collected from the ZnO nanorods and the ZnO@C@Si nanorods on the Ni foam. The crystalline peaks are assigned to hexagonal ZnO (JCPDS card no. 80-0074). (b) EDX spectrum of the ZnO@C@Si nanorod array on Ni foam.

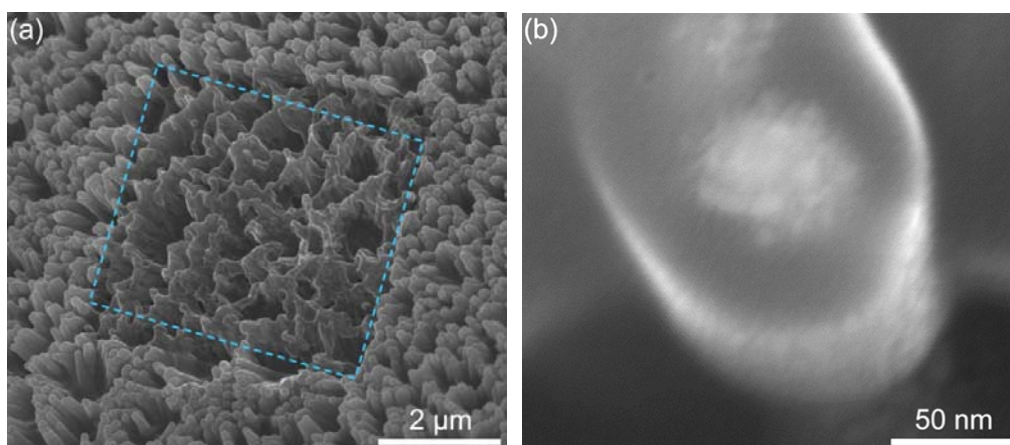


Figure S3. (a) Low- and (b) high-magnification SEM images of the ZnO@C@Si nanorods after removal of the top layer by FIB, providing a cross-sectional image. The dashed box in (a) indicates the FIB-milled region. In (b), the cross-section of a single nanorod is shown.

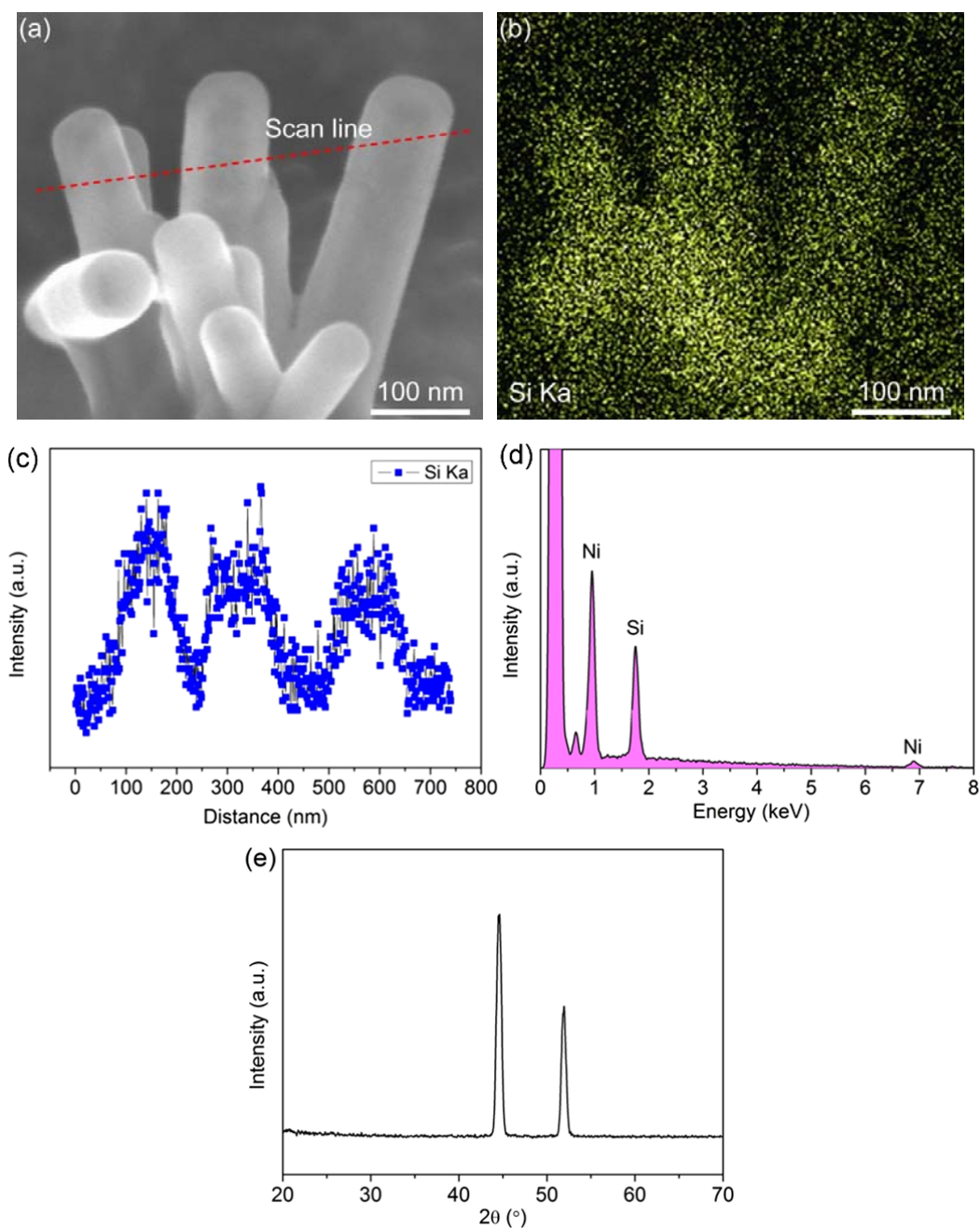


Figure S4. (a) SEM image of the C@Si@C nanotube array after ZnO etching. The dashed red line indicates the line-scanning position used for (c). (b) Elemental mapping of Si K α . The Si signal matches well with the position of the nanotubes in (a). (c) Distribution of Si along the line in (a). (d) EDX spectrum and (e) XRD pattern of the sample. In EDX spectrum, Ni and Si are detected without the appearance of Zn, indicating that the ZnO core has been etched completely. No ZnO peaks are observed in the XRD.

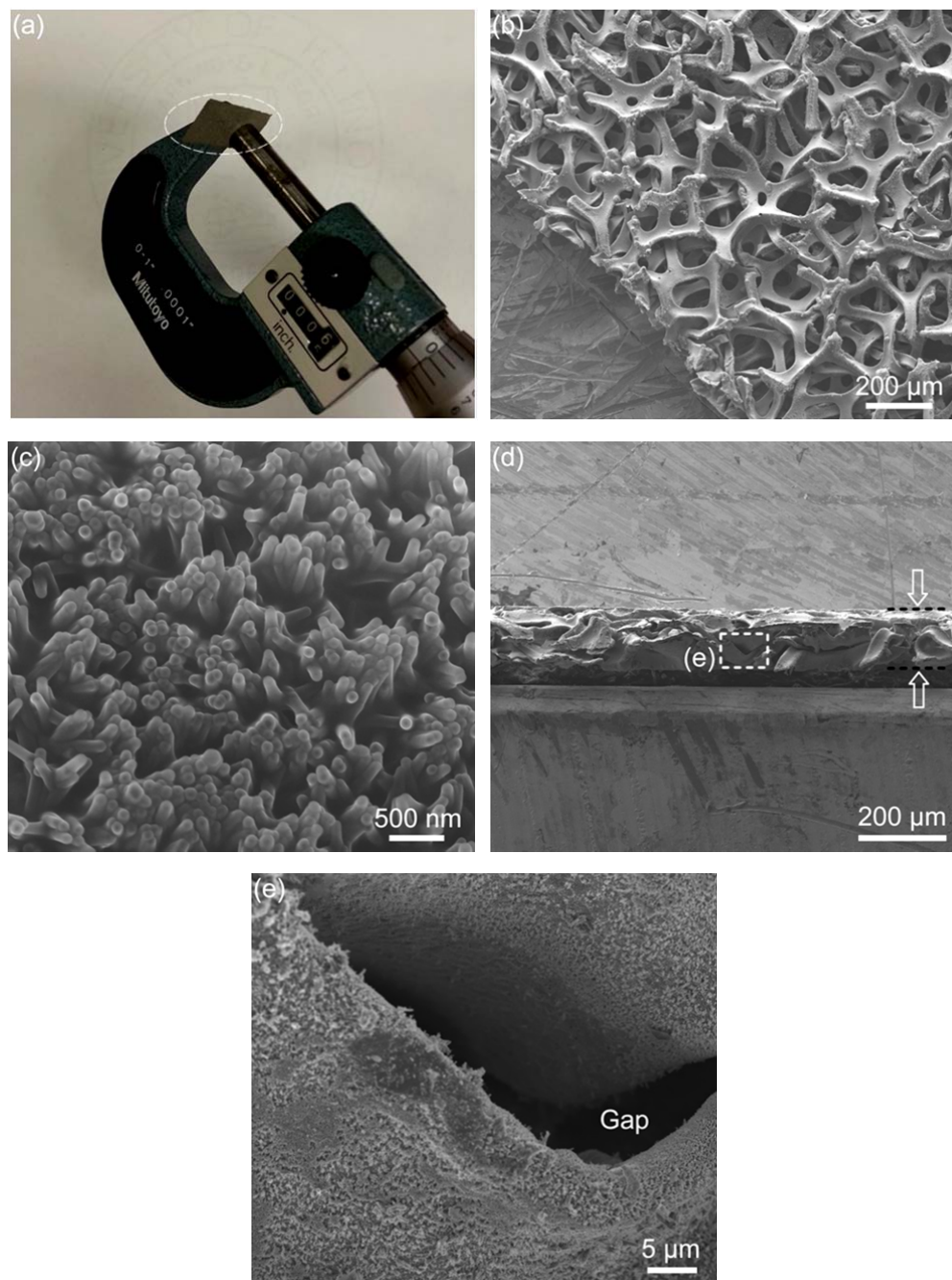


Figure S5. (a) Photo of a C@Si@C nanotube array grown Ni foam after thickness compression (measured in the micrometer). (b), (c) top and (d), (e) cross-sectional SEM images of the compressed samples. The Ni foam, as well as the nanotube array, retains the initial structure without cracking after compression to 150 μm . From the cross-sectional SEM image shows porosity remain in the compressed structure, in which the nanotube array remains undamaged.

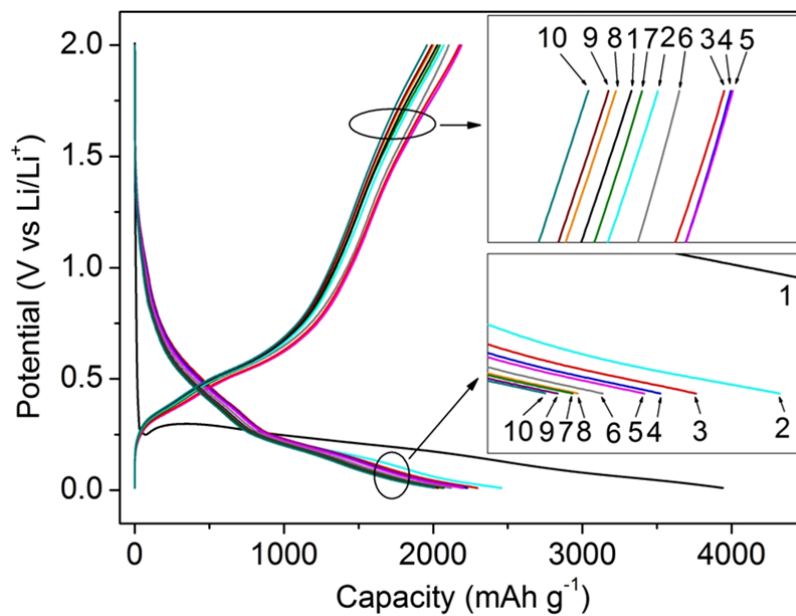


Figure S6. Electrochemical properties of the C@Si@C nanotube array on the compressed electrode over the first 10 cycles. Galvanostatic charge/discharge at a rate of 0.2C.

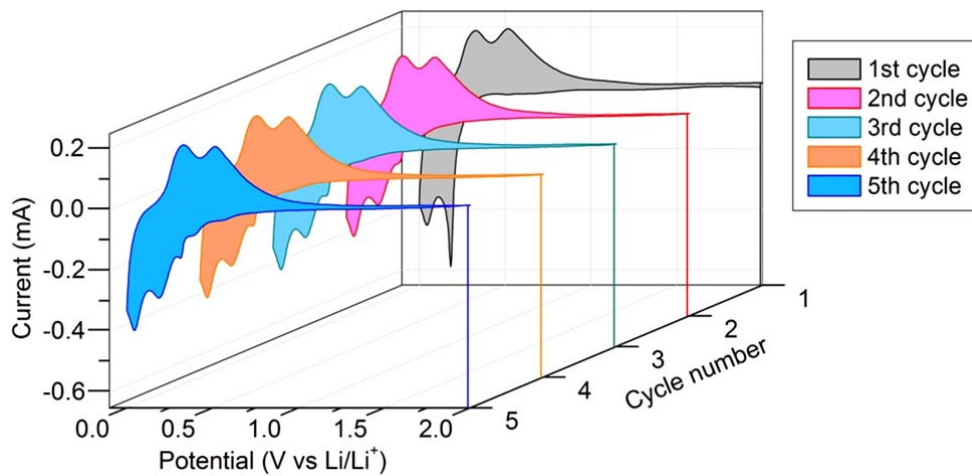


Figure S7. CV curves of the C@Si@C nanotube array over the potential range of 0.0 to 2.0 V at a rate of 0.1 mV s⁻¹.

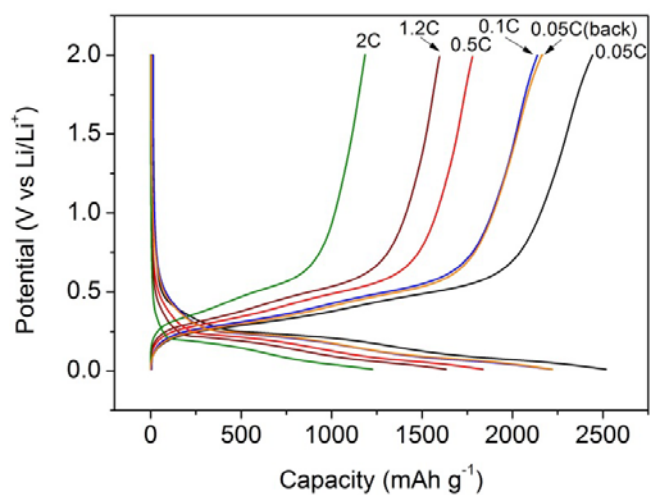


Figure S8. Galvanostatic charge/discharge curves of the C@Si@C nanotube electrode from 0.05C to 2C. The 0.05C (back) confirms that the current density returns to initial 0.05C capacity after 2C rate cycling.

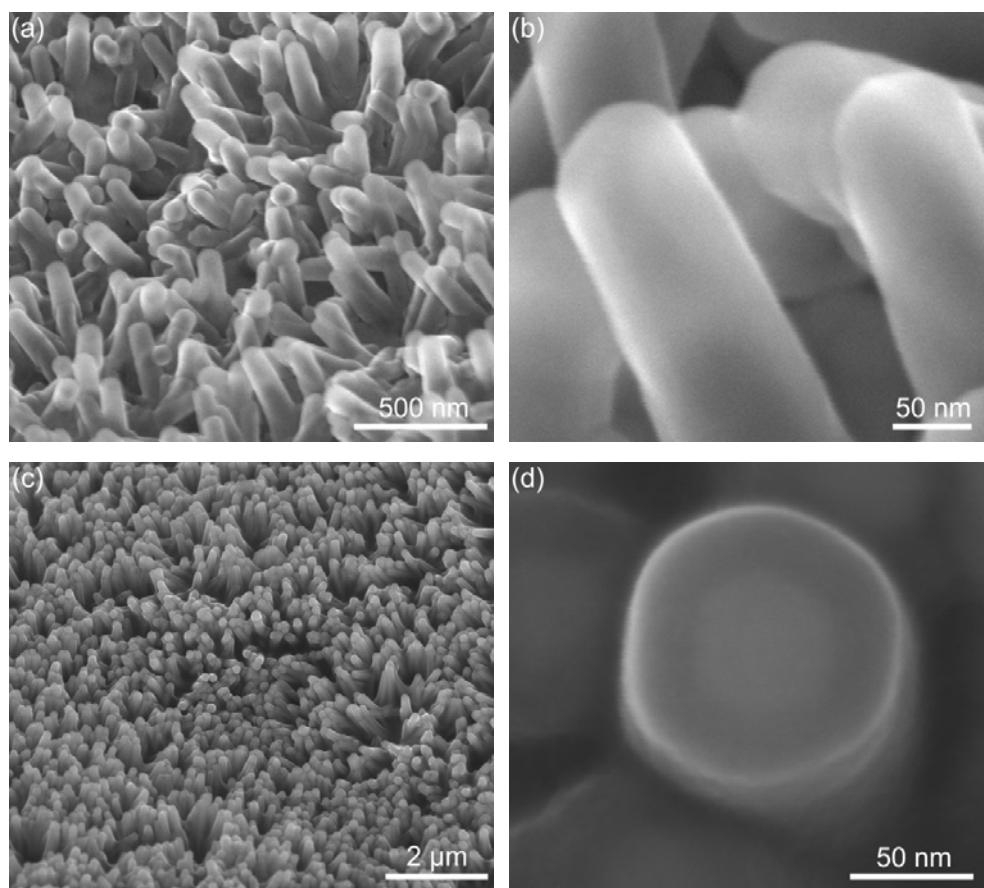


Figure S9. SEM images of (a), (b) the Si nanotube array and (c), (d) the ZnO@C@Si@C nanorod array.

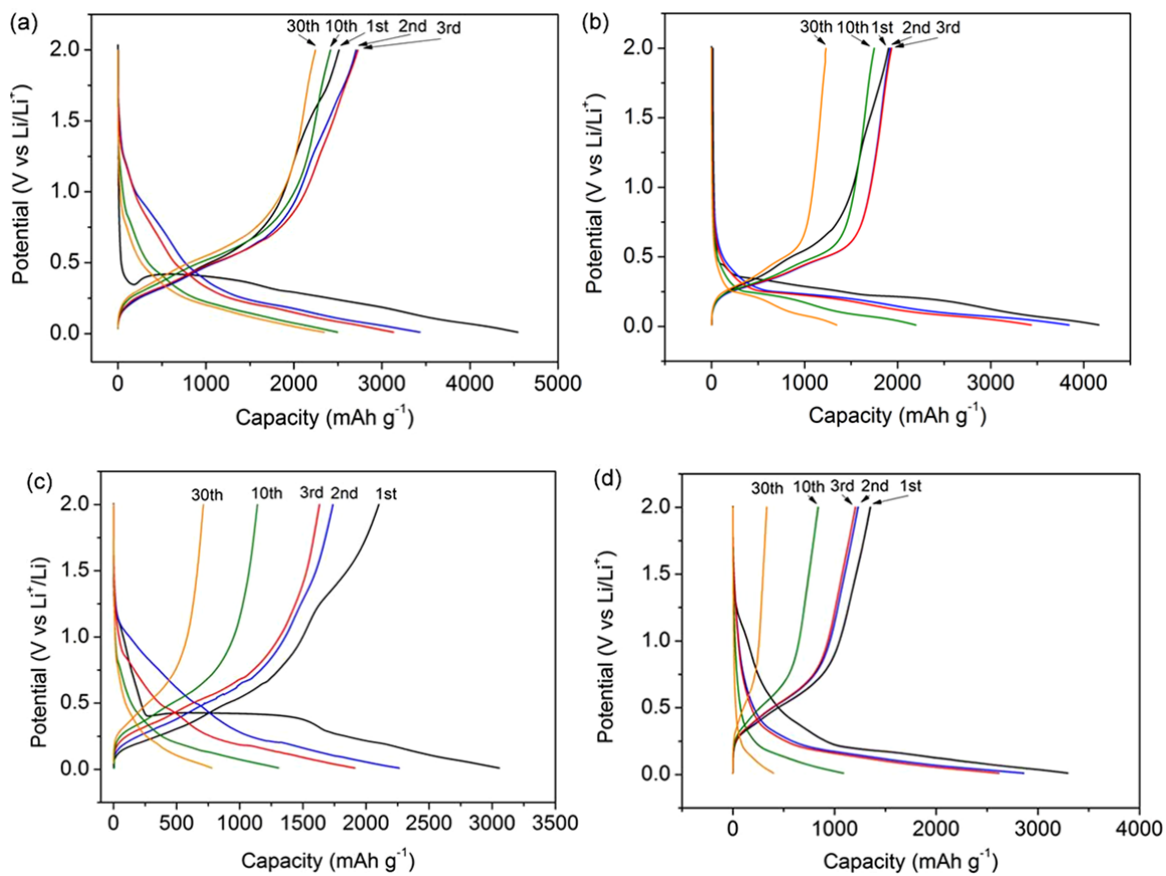


Figure S10. Galvanostatic charge/discharge curves (at a rate of 0.08C) of (a) the C@Si@C nanotube array, (b) Si nanotube array, (c) ZnO@C@Si@C nanorods array, and (d) Si thin film on Ni foam.

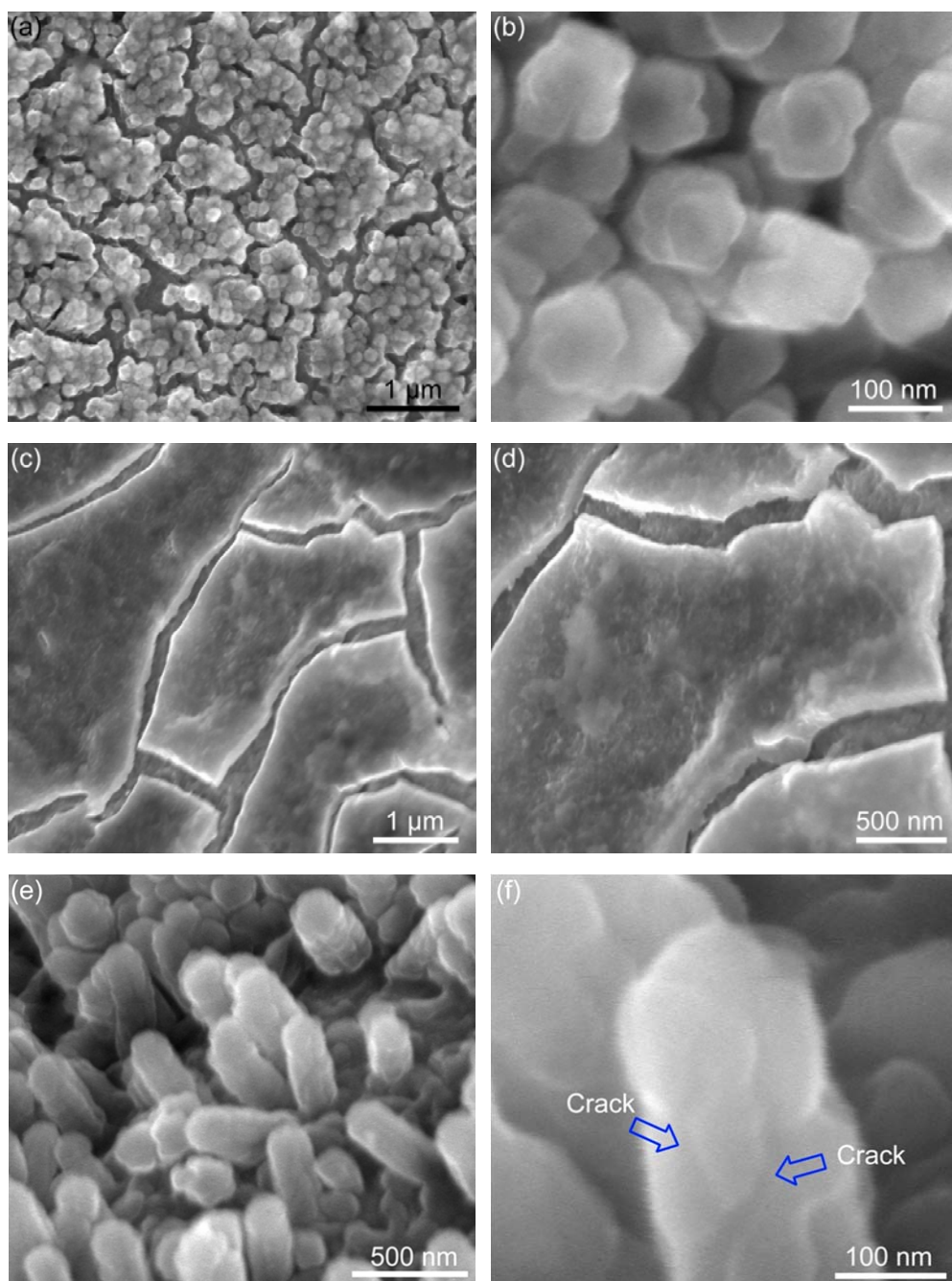


Figure S11. Post-cycled electrodes: SEM images of (a), (b) the Si nanotube array, (c), (d) the Si thin film on Ni foam, and (e), (f) the ZnO@C@Si@C nanorod array after cycling at 0.08C over 30 cycles.

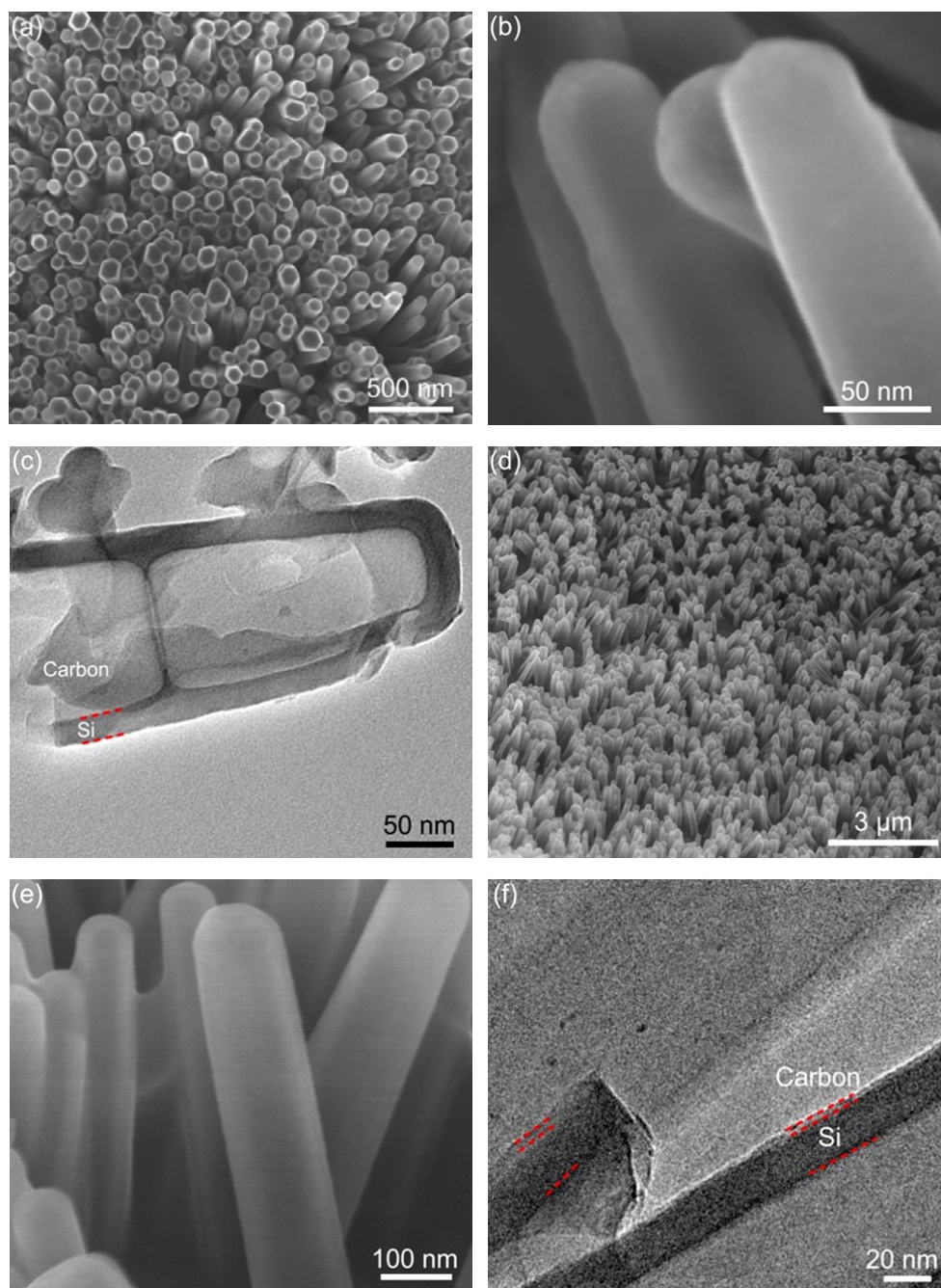


Figure S12. (a), (b) SEM images of the C@Si nanotube array; (c) TEM image of the C@Si nanotube; (d), (e) SEM images of the Si@C nanotube array; and (f) TEM image of the Si@C nanotube.

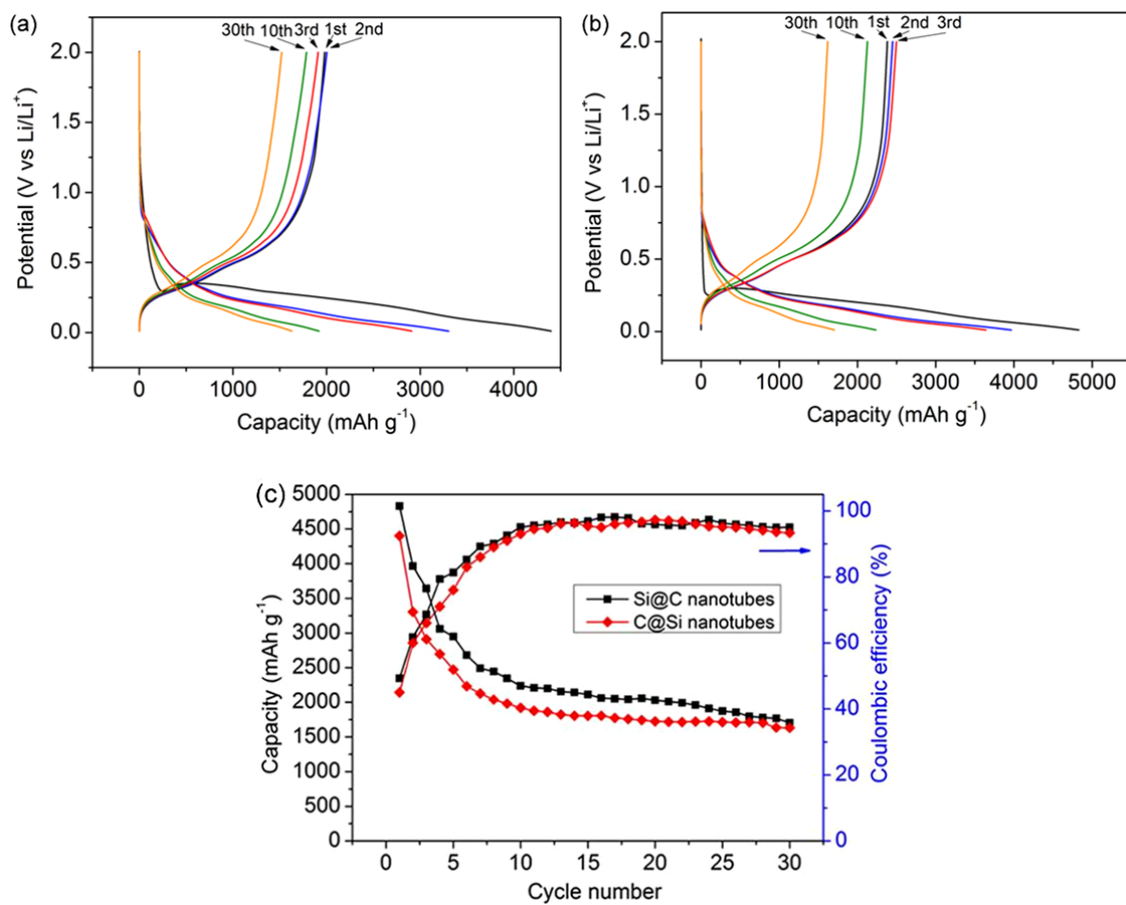


Figure S13. Galvanostatic charge-discharge curves of the (a) C@Si and (b) Si@C nanotube array. (c)

The corresponding discharge capacity and Coulombic efficiency.

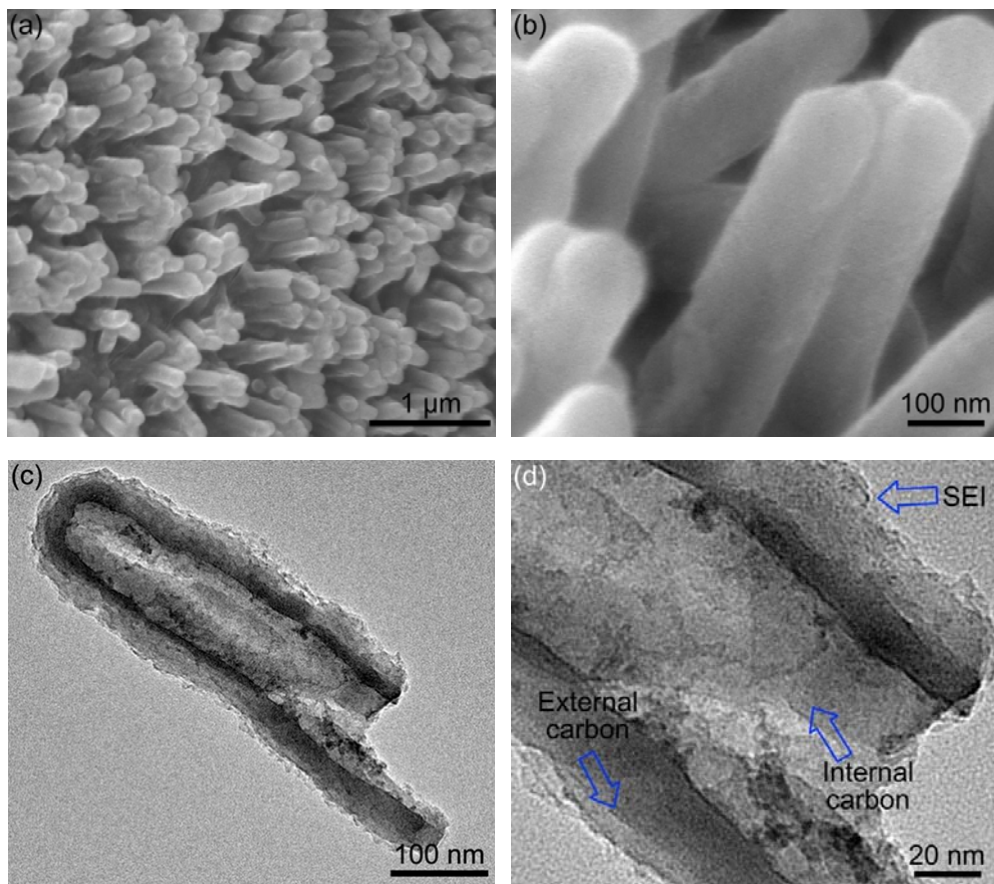


Figure S14. (a), (b) SEM and (c), (d) TEM images of the C@Si@C nanotubes after cycling at 0.08C over 30 cycles. The internal carbon layer, external carbon, and SEI are marked in (d).

Impedance measurements. The charge and discharge kinetics of the C@Si@C nanotubes were investigated *via* electrochemical impedance spectroscopy at different charge and discharge states. As can be seen from Fig. S19a, all Nyquist plots show a compressed semicircle in the high frequency region and an inclined tail in the low frequency region. The compressed semicircle in the high frequency is assigned to the resistance of SEI and the charge transfer impedance at the interface between electrode and electrolyte interface, while the inclined line at low frequencies is attributed to the Li-ion diffusion processes within the electrode¹⁻³. As the electrode was charged from 0.2 to 0.6, 1.2, and 1.8 V, the diameter of each semicircle increases, indicating that the resistance of the electrode increases with extraction of Li-ions (delithiation). Fig. S19b shows the impedance stability of the electrode after 10 charge/discharge cycles at a rate of 0.08C. The impedance measurements during these charge and discharge processes show similar profiles, indicating a stable surface chemistry (*e.g.* the SEI layer) and near-constant Li-ion diffusion coefficient.

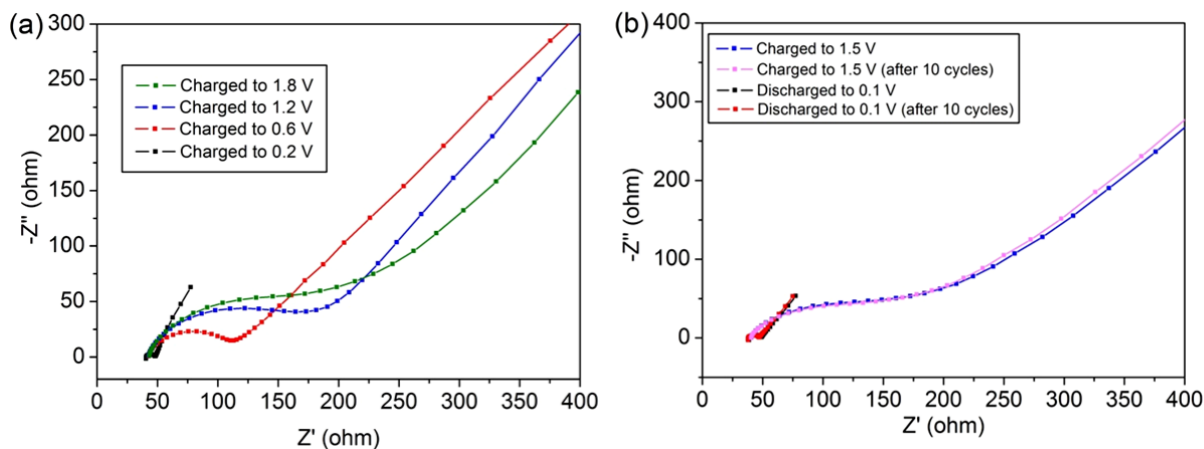


Figure S15. (a) Nyquist plots of electrodes charged to 0.2, 0.6, 1.2, and 1.8 V. (b) Nyquist plots of the electrode before and after charge/discharge for 10 cycles.

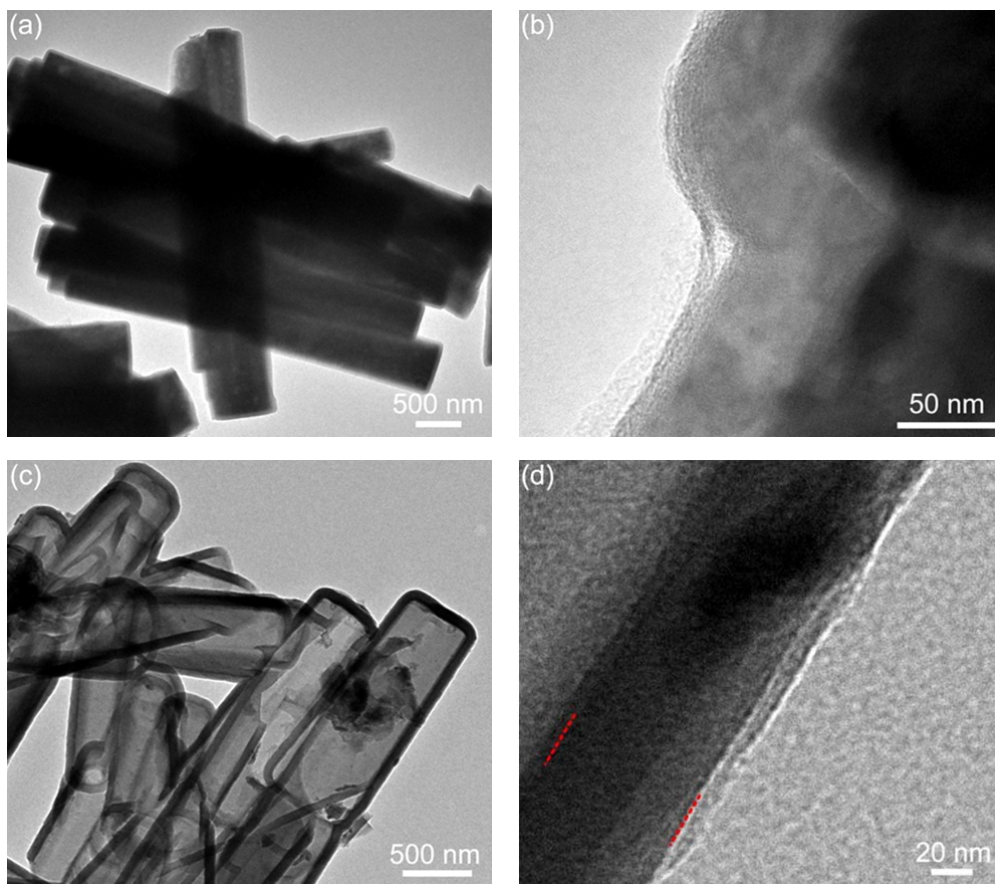


Figure S16. TEM images of (a), (b) the ZnO@C@Si@C nanorods with a large ZnO core, and (c), (d) the C@Si@C nanotubes after ZnO removal for *in-situ* SEM observation.

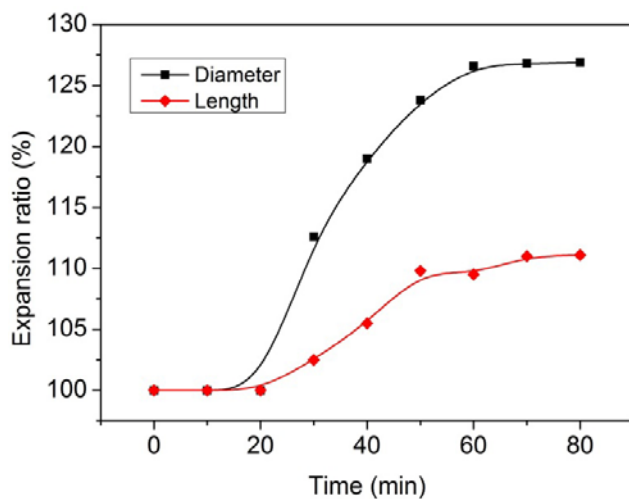


Figure S17. Relationship of expansion ratio *versus* time during the first lithiation process of the C@Si@C nanotubes.

Table S1. Diameter and length expansion ratios in the first lithiation-delithiation and the second lithiation processes of the C@Si@C nanotubes.

	Diameter (nm)	Percentage (%)	Length (nm)	Percentage (%)
Initial size	820.1	–	4654.0	–
First lithiation	1045.3	127	5154.3	111
First delithiation	878.9	107	4876.7	105
Second lithiation	1037.0	126	5154.8	111

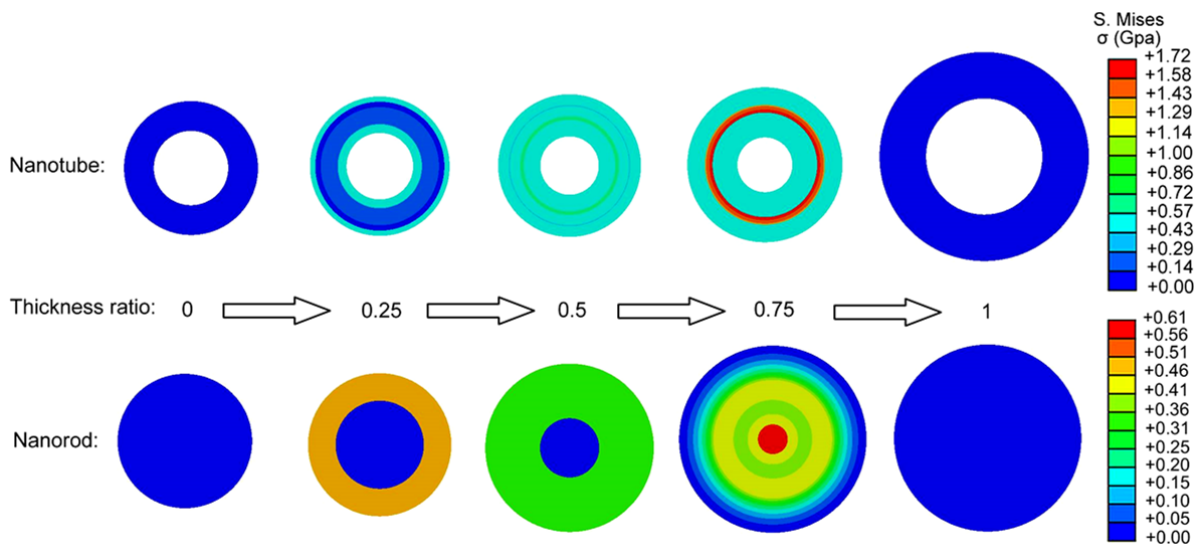


Figure S18. Nanotubes and nanorod von Mises stress contours during lithiation.

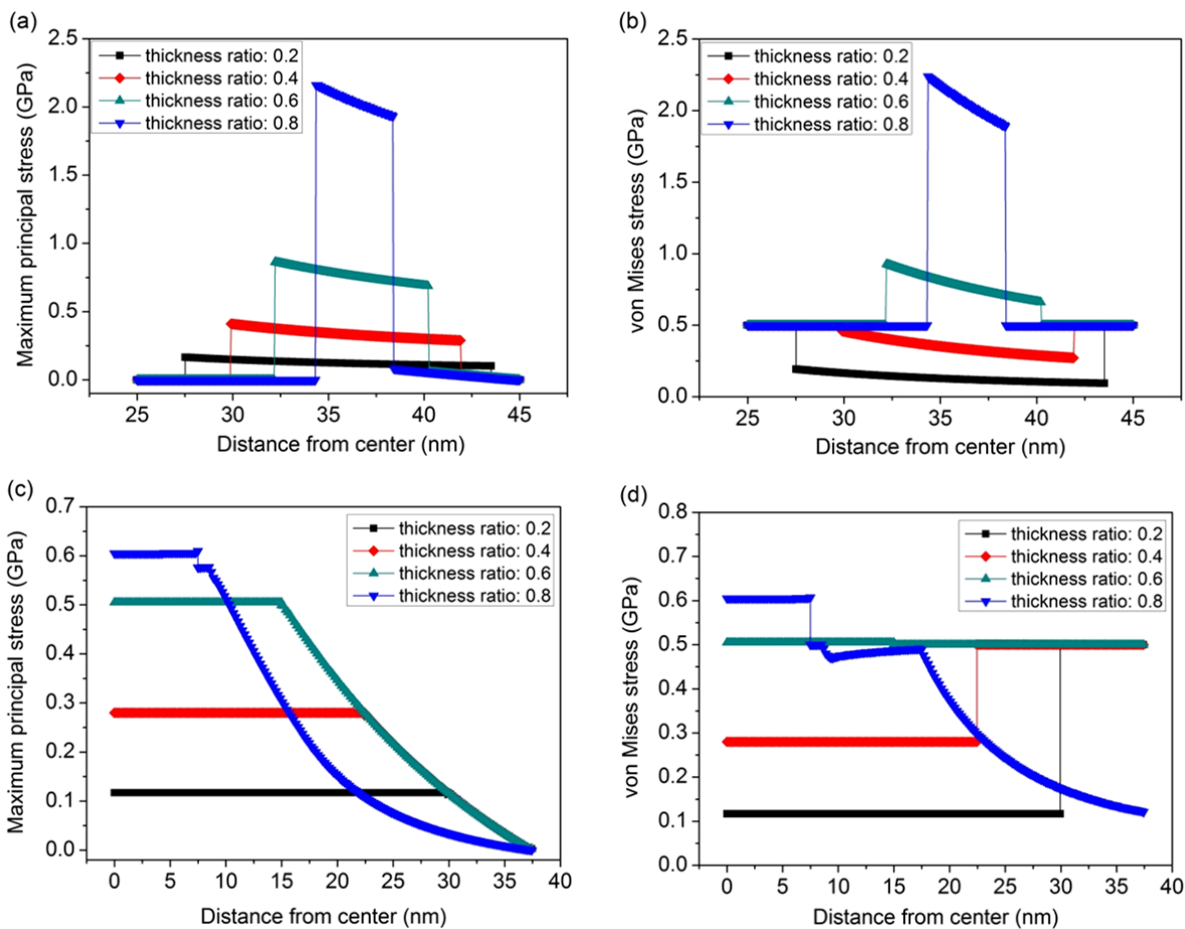


Figure S19. (a) the maximum principal stresses and (b) the von Mises stresses in nanotubes. (c) the maximum principal stresses and (d) the von Mises stresses in nanorods.

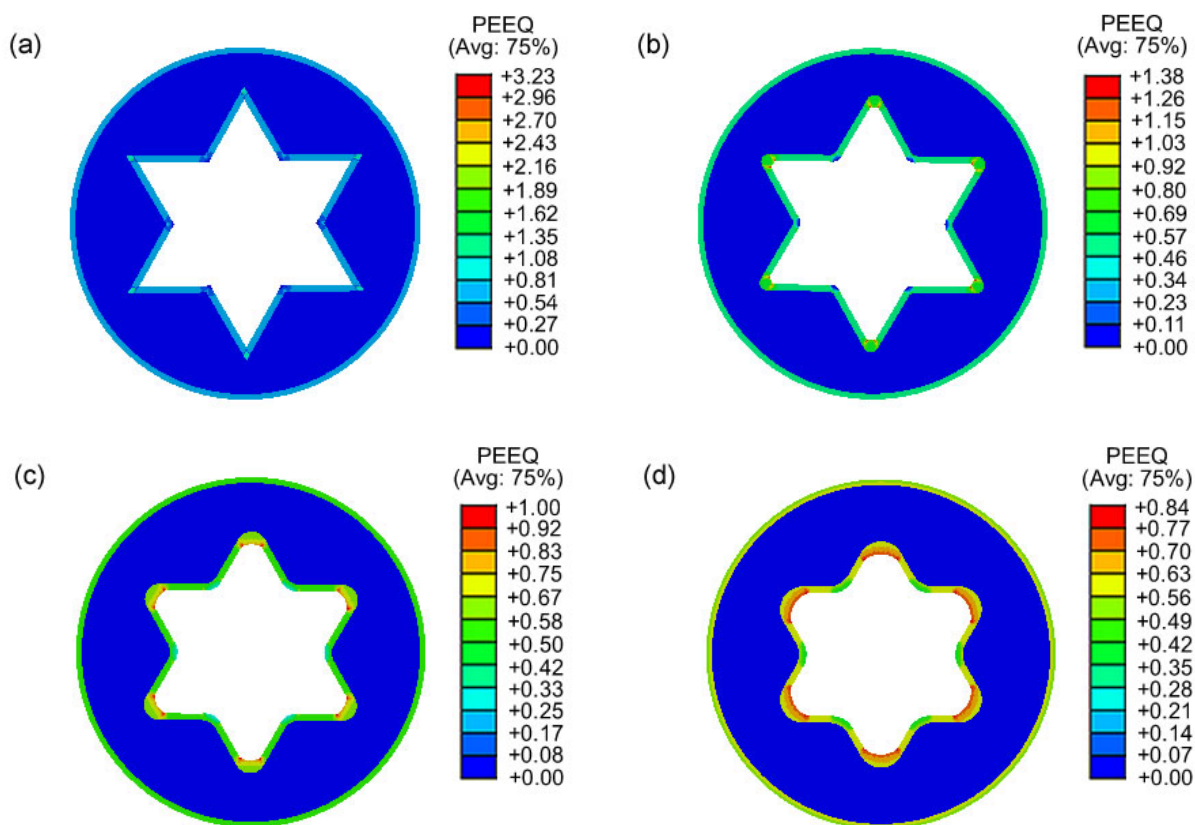


Figure S20. Plastic strain contours of nanotubes with (a) a hexagram shaped inner pore. In (b), each angle is smoothed into a 2 nm radius arc. In (c), each angle is smoothed into a 4 nm arc. In (d), each angle is smoothed into an 8 nm arc.

Relationship between thickness ratio and degree of lithiation (state of charge). The thickness ratio is defined as the thickness of the silicon which has been lithiated, divided by the initial thickness of the silicon nanorod or nanotube. We assume the rods are long relative to their diameter, and thus the fraction of the area of the silicon which has been lithiated, is the same as the fraction of the total volume of the silicon which has been lithiated. The thickness ratio can be converted to a degree of lithiation (same as the state of charge), as follows:

Si nanorods

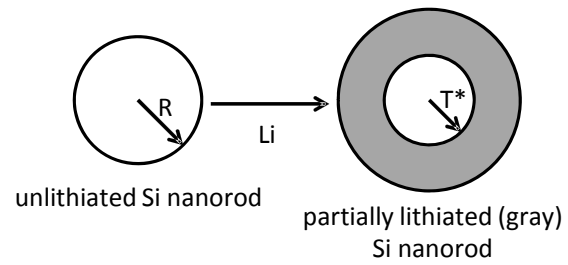
R = Initial Si nanorod diameter

T* = Radius of Si which has not been lithiated

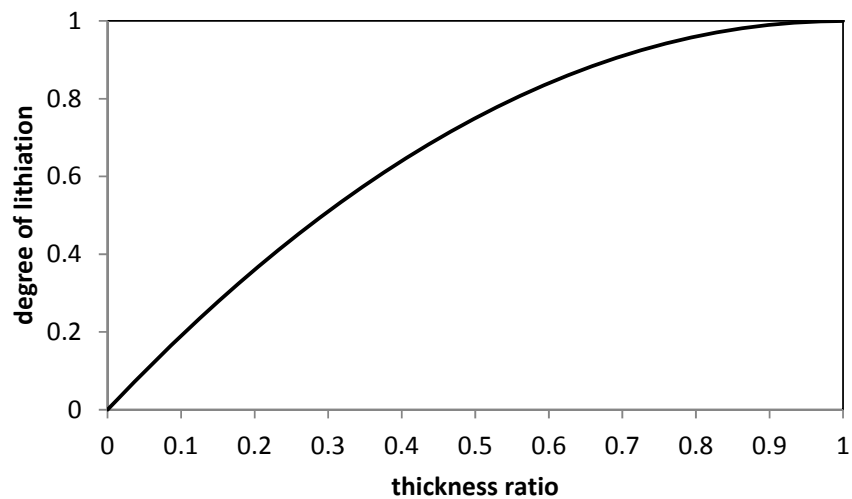
$$\text{Thickness ratio} = \frac{1 - T^*}{R}$$

Degree of lithiation = (initial Si area - remaining Si area)/initial Si area

$$\begin{aligned} &= \frac{\pi R^2 - \pi T^{*2}}{\pi R^2} \\ &= \frac{R^2 - T^{*2}}{R^2} \end{aligned}$$



The degree of lithiation vs. thickness ratio can then be plotted as follows:

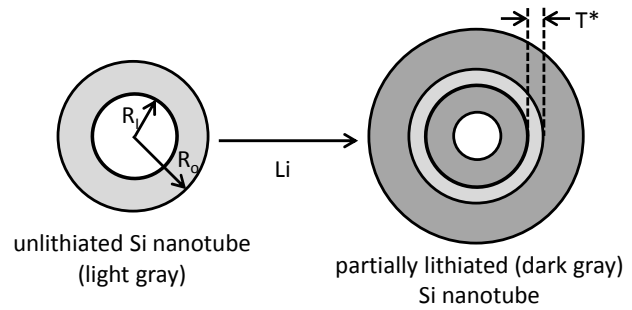


Si nanotubes

R_o = Outside Si nanotube diameter

R_i = Inside Si nanotube diameter

T^* = Thickness of Si which has not been lithiated



We assume the Si lithiation on the inside and outside of the tube occurs at the same rate, which may not be fully accurate.

$$\text{Thickness ratio} = \frac{R_o - R_i - T^*}{R_o - R_i}$$

Degree of lithiation = (initial Si area - remaining Si area)/initial Si area

$$\begin{aligned} &= \frac{\pi R_o^2 - \pi R_i^2 - \pi \left(R_o - \frac{1}{2}(R_o - R_i - T^*)\right)^2 - \pi \left(R_i + \frac{1}{2}(R_o - R_i - T^*)\right)^2}{\pi R_o^2 - \pi R_i^2} \\ &= \frac{R_o^2 - R_i^2 - \left(R_o - \frac{1}{2}(R_o - R_i - T^*)\right)^2 - \left(R_i + \frac{1}{2}(R_o - R_i - T^*)\right)^2}{R_o^2 - R_i^2} \\ &= \frac{R_o - R_i - T^*}{R_o - R_i} \quad (\text{which is the same as the thickness ratio}) \end{aligned}$$

Thus, in the nanotube geometry, the thickness ratio is the same as the degree of lithiation (the state of charge).

REFERENCE

- (1) Cetinkaya, T.; Uysal, M.; Guler, M. O.; Akbulut, H.; Alp, A. *Powder Technol.* **2014**, 253, 63–69.
- (2) Tao, H. C.; Huang, M.; Fan, L. Z.; Qu X. H. *Electrochim. Acta* **2013**, 89, 394–399.
- (3) Kwon, E.; Lim, H. S.; Sun, Y. K.; Suh, K. D. *Solid State Ionics* **2013**, 237, 28–33.